Synthesis, Simulation and Experimental Verification of a Maximum Power Point Tracker from Nonlinear Dynamics

Yan Hong Lim (y.lim@eim.surrey.ac.uk)
David C. Hamill (d.hamill@surrey.ac.uk)
Surrey Space Centre
University of Surrey, Guildford, United Kingdom, GU2 7XH

***Abstract* — A simple but robust maximum power point tracker (MPPT) is proposed, derived from nonlinear dynamics. The maximum power point (MPP) inherently becomes the global attractor of the system, ensuring optimum operation under transient and steady state conditions. The control algorithm is first synthesised and implemented, supported by PSpice simulations and verified by experiments. The results confirm good tracking efficiency and rapid response to parameter changes.**

In addition, a two-dimensional approximate stroboscopic map was also found that adequately describes the system's global attractor and its fundamental dynamics at the MPP. This was confirmed experimentally from a return map featuring one of the state variables.

I. INTRODUCTION

The amount of power obtained from a photovoltaic array depends on the operating voltage of the array. From its typical *v–i* and *v–p* characteristics (Fig. 1(a) and (b) respectively), there exists a unique operating point $v = V_{mpp}$, known as the maximum power point (MPP) that delivers the maximum available power P_{max}. When operated at the MPP, the array is best utilised.

The MPP of a photovoltaic array varies with illumination, temperature, radiation dose, ageing and other effects. By denoting these time-varying parameters as $(\theta_1, \theta_2, \cdots)$ and from the chain rule, *dp/dt* can be written as

$$\frac{dp}{dt} = \frac{\partial p}{\partial v}\frac{\partial v}{\partial t} + \underbrace{\frac{\partial p}{\partial \theta_1}\frac{\partial \theta_1}{\partial t} + \frac{\partial p}{\partial \theta_2}\frac{\partial \theta_2}{\partial t} + \ldots}_{\text{confusion/noise}} \qquad (1)$$

It is the noise term in (1) that makes an accurate estimation of V_{mpp} non-trivial, and requires *v* to be continuously adjusted.

Most maximum power point trackers (MPPTs) are based on the concept of '*perturb and observe*' (P&O) — see [1] and references therein. The impressed voltage is varied in steps, and the power output is monitored. If the power increases, another step is taken in the same direction; otherwise, the direction is reversed.

Although implementation is simple, often by a microprocessor, it can be slow and become 'confused' when the MPP moves rapidly [2]. Other alternatives to P&O were recently suggested [3][4].

In this paper, a new control strategy for MPP tracking that draws on nonlinear dynamics concepts is proposed. The MPP becomes inherently the system's only *attractor*, exhibiting a global *basin of attraction*. Hence, the system is therefore guaranteed to autonomously track the MPP under steady state and transient conditions.

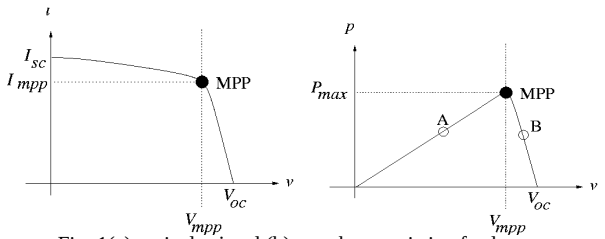

Fig. 1(a) typical *v-i* and (b) *v-p* characteristic of solar array

II. SYNTHESIS OF THE CONTROL ALGORITHM

We first concentrate on an unvarying *v-p* characteristic that implies neglecting the noise terms in (1). Differentiating the *v–p* curve of Fig. 1(b) produces Fig. 2(a). The MPP (V_{mpp}, P_{max}) is located where $dp/dv = 0$. It is usually safe to assume that the *v–p* characteristic is unimodal, so the MPP is a global maximum. Therefore,

$$\frac{\partial p}{\partial v} = \begin{cases} > 0 & \text{if} \quad v < V_{mpp} \\ = 0 & \text{if} \quad v = V_{mpp} \\ < 0 & \text{if} \quad v > V_{mpp} \end{cases} \qquad (2)$$

An obvious control strategy would be the following: if $\partial p / \partial v > 0$, we deduce $v < V_{mpp}$, so increase *v* so that operation moves towards V_{mpp}; on the other hand, if $\partial p / \partial v < 0$, then $v > V_{mpp}$, so decrease *v* instead; but if $v = V_{mpp}$, then hold *v* constant, as we are at the MPP. In differential form:

$$\frac{dv}{dt} = \dot{v} = \begin{cases} > 0 & \text{if} \quad v < V_{mpp} \\ = 0 & \text{if} \quad v = V_{mpp} \\ < 0 & \text{if} \quad v > V_{mpp} \end{cases} \qquad (3)$$

The simplest function conforming to (3) is $\dot{v} = -k(v - V_{mpp})$, where *k* is a positive coefficient associated with speed; the larger *k*, the faster the dynamic response. This function is shown in Fig. 2(b). However, any function complying with (3) would do, for instance that of Fig. 2(c), which even has a discontinuity at $v = V_{mpp}$. Observing that (2) and (3) have similar forms, we see that a simple control strategy is to make $\dot{v} = k\partial p / \partial v$, where $k > 0$.

To achieve this, we need information about $\partial p / \partial v$. Neglecting noise terms in (1), we have $\partial p / \partial v = (dp/dt)/(dv/dt) = \dot{p} / \dot{v}$. Therefore, a suitable control algorithm

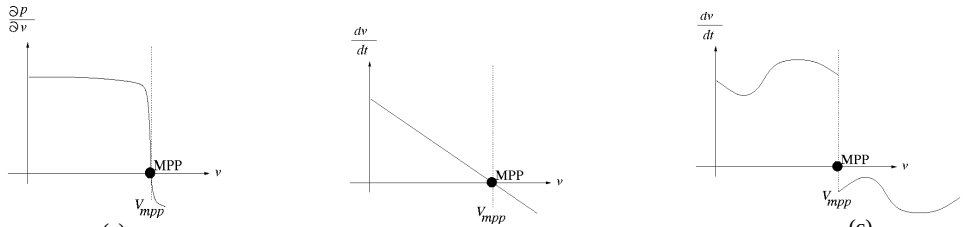

Fig. 2: (a) typical $\partial p/\partial v$-v characteristic of photovoltaic array, (b) simple (c) alternative characteristic making V_{mpp} an attractor

would seem to be $\dot{v} = k\dot{p}/\dot{v}$. But there are problems. First, this equation contains an algebraic loop, as $\dot{v}$ appears on both sides. This would manifest itself in practice as a high frequency oscillation. Second, analogue dividers are undesirable components, as they have many imperfections. Finally, a division-by-zero singularity occurs when $\dot{v}$ becomes zero: this happens at $v = V_{mpp}$, a very unfortunate location! (Note that P&O avoids this problem by making $\dot{v}$ always non-zero). Rearranging the equation into the form $\dot{v}^2 = k\dot{p}$ does not help either, because squaring $\dot{v}$ destroys the vital information of its sign. Other transformations are equally unhelpful.

The whole issue lies with the use of $\dot{p}/\dot{v}$ on the right-hand side (RHS) of the control equation. However, we can resolve this since all that really matters is its sign (as used in P&O). Using the normal definition of the signum function (sgn$x$ = –1 if x < 0, 0 if x = 0, +1 if x > 0), we may write $\mathrm{sgn}(\dot{v}) \leftarrow \mathrm{sgn}(\dot{p}/\dot{v})$ where '←' denotes the assignment of information held by the RHS to the left-hand-side (LHS) of the control equation.

Unfortunately, this is still not satisfactory, since the RHS can be zero even if we are not at the MPP, and the singularity issue is still not resolved. However, this objection can be countered by employing a modified signum function which never returns a zero value: Sgn x = –1 if x < 0, +1 if $x \geq 0$. We first rewrite the RHS as $\mathrm{sgn}(\dot{p}/\dot{v}) \equiv \mathrm{sgn}\,\dot{p}/\mathrm{sgn}\,\dot{v}$. We then introduce the modified signum function and transform $\mathrm{sgn}\,\dot{p}/\mathrm{sgn}\,\dot{v} \Rightarrow \mathrm{Sgn}\dot{p}/\mathrm{Sgn}\dot{v}$. The difference between the LHS and RHS of this equation, in practice, is negligible. To avoid using analogue dividers, we further rewrite $\mathrm{Sgn}(\dot{p})/\mathrm{Sgn}(\dot{v}) \equiv \mathrm{Sgn}(\dot{p})\mathrm{Sgn}(\dot{v})$. Hence, our final control equation becomes

$$\mathrm{Sgn}(\dot{v}) \leftarrow \mathrm{Sgn}(\dot{p})\mathrm{Sgn}(\dot{v}) \qquad (4)$$

The RHS of the control equation contains information on whether $\dot{v}$ should be increased or decreased to approach the MPP. Because the Sgn(·) function has a discontinuity at the MPP, the system will not settle to the MPP but will instead oscillate around it. This implies that the MPP cannot be an equilibrium point, but must be a more complex type of attractor.

III. PRACTICAL REALISATION OF THE CONTROL EQUATION

For illustration, we consider the system whose power stage comprises a solar array, a buck dc-dc converter and a battery load as shown in Fig. 3.

A. Implementation of the RHS of the Control Equation

The RHS of the controller can be implemented simply using two differentiators, two comparators and an analogue multiplier to evaluate $p = vi$. The differentiator can be realised by a first-order high pass filter. The multiplication of the two signs, expressed as booleans, can be performed using an exclusive-or gate (XOR). The output of the XOR yields a binary signal, indicating whether v should be increased or decreased.

B. Implementation of the LHS of the Control Equation

In Fig. 3, to increase the impressed voltage across the array, we can open switch S so that the capacitor charges up. To decrease the voltage, the capacitor is made to discharge by closing the switch. This opening or closing of the switch can be made to correspond correctly to the output from the XOR. This output is then sampled by a D-type latch clocked at a constant frequency $1/T_s$, whose output provides the signal to drive the switch. This latch is incorporated (a) to prevent high frequency switch chattering and (b) to minimise the effects of unavoidable interference generated by the buck converter's switching action. This interference occurs immediately after a clock transition, and is over before the next, so the latch never samples it. The overall control equation is thus satisfied.

C. Principle of Operation of Controller

The qualitative operation of the controller is summarised in Table 1. Each comparator has two states, so there are four basic modes.

Consider point A in Fig. 1(b), where $v < V_{mpp}$. If v decreases, p also decreases, retreating from the MPP. To counter this, the controller opens the switch so that C can charge. This corresponds to row 2 of Table 1. With the switch open, v now increases towards V_{mpp}, increasing p and approaching the MPP as desired (row 1).

On the other hand, if $v > V_{mpp}$ (point B), the controller takes the reverse action, decreasing v towards the MPP by closing

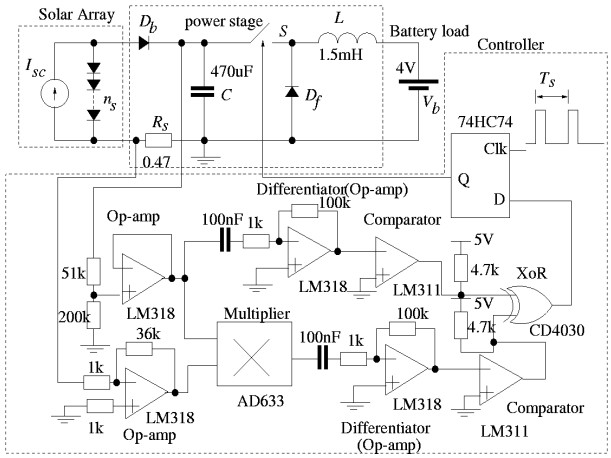

Fig. 3: Schematic of proposed MPPT

the switch (rows 3 and 4). Hence, the controller creates an inherent attractor at the MPP. However, it is impossible to reach the MPP exactly, because if $v = V_{mpp}$, the switch opens, making v increase. But this subsequently leads to the switch closing, making v decrease; thus the voltage wanders around V_{mpp}.

IV. SIMULATION AND EXPERIMENTAL RESULTS

A constant current source shunted by a string of n_s diodes is used to mimic a real array for ease of simulating variations in its characteristics, e.g. due to illumination and temperature.

The following parameters are used: I_{sc} = 0.25~0.75A, n_s = 12~20 diodes, V_b = 4V, L = 1.5mH, C = 470μF, T_s = 50μs, T_d = 100μs. The system in Fig. 3 has been simulated with PSpice and also experimentally constructed.

Table 1: Principle of operation of controller

			Comparator output				
Condition	$\dot{p}$	$\dot{v}$	X_p	X_v	S	Switch	v
$v \le V_{mpp}$	> 0	> 0	1	1	0	opens	increases
$v \le V_{mpp}$	≤ 0	≤ 0	0	0	0	opens	increases
$v > V_{mpp}$	> 0	≤ 0	1	0	1	closes	decreases
$v > V_{mpp}$	≤ 0	> 0	0	1	1	closes	decreases

A. Dynamic Performance

A variety of extreme scenarios were conducted to establish the MPPT's dynamic performance. Two extreme cases are presented here. For example, with a full string of 20 diodes, I_{sc} was abruptly switched from 0.25A to 0.75A to simulate an increase in illumination. Fig. 4(b) shows the settling time is less than ~5ms. Fig. 4(d) experimentally plots the array voltage against power. It is evident that the trajectory converges to the new MPP, as it traces out a typical nonlinear v–p curve, climbing to its peak and oscillating there. (A thickened patch is evidence of this.) The experimental

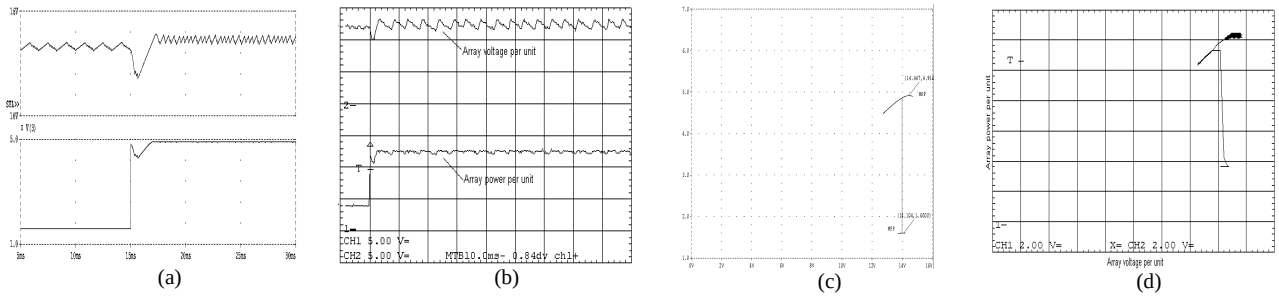

(a) (b) (c) (d)

Fig. 4: (a) PSpice simulation, top: array voltage, bottom: array power, (b) experimental time trajectory; (c) PSpice simulated, (d) experimental voltage-power characteristic when I_{sc} switched from 0.25A to 0.75A with 20 diodes

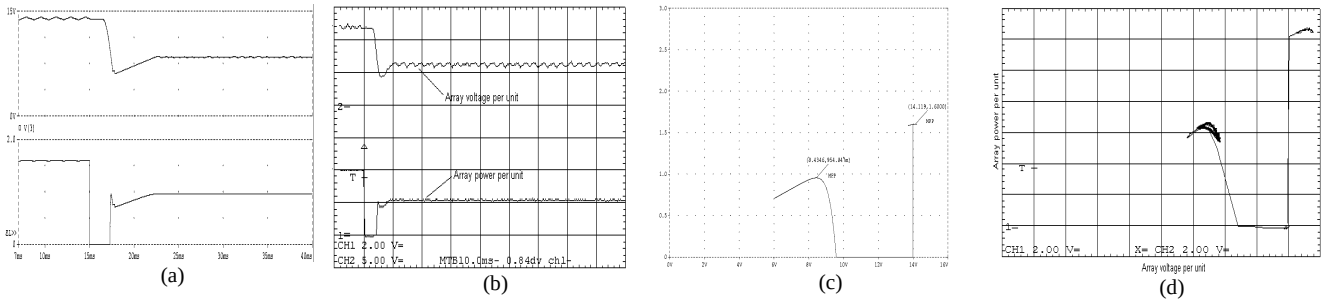

(a) (b) (c) (d)

Fig. 5: (a) PSpice simulation, top: array voltage, bottom: array power, (b) experimental time trajectory, (c) PSpice simulated, (d) experimental voltage-power characteristic when n_s is switched from 20 to 12 with I_{sc} = 0.25A

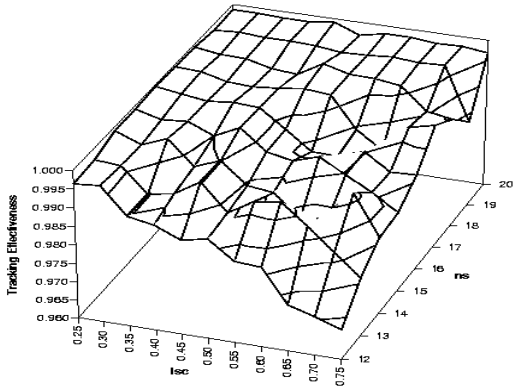

Fig. 6: Experimental tracking effectiveness against number of diodes (n_s) and array's short-circuit current (I_{sc})

waveforms also agree well with the PSpice generated waveforms of Fig. 4(a) and (c). To simulate a change in temperature affecting the array voltage, I_{sc} is held at 0.25A while the number of diodes is switched from 20 to 12. Fig. 5(b) shows the reacquisition time to be less than 10ms. Other scenarios were tried, and in all cases, the MPP was reacquired within a few milliseconds.

Because practical solar arrays incorporate a blocking diode D_b to prevent reverse current, when V_{oc} reduces rapidly, it is possible that v could exceed V_{oc}, making $p = 0$. The controller becomes confused because $\dot{p} = 0$ and a latchup could occur.

This is easily prevented by imposing an operational boundary for MPP seeking: if $p < P_{min}$ (a threshold value), we set the switch to close and capacitor C discharges, reducing v. This is easily implemented using just another comparator and gate (not shown in Fig. 3). P_{min} should be small, to allow MPP tracking at low illumination levels.

B. Static Performance

A figure of merit for the static performance of an MPPT is its tracking effectiveness, defined as P/P_{max} (ideally unity), where P is the mean power extracted from the array and P_{max} is the maximum available power under the same conditions.

With the controller disabled, and the buck converter driven by a pulse generator at a frequency $1/T_s$, the value of P_{max} = max (vi) was found by manual adjustment of the duty ratio. The controller was then enabled, and $P = vi$ was measured. Over most of the experimental range, the tracking effectiveness was better than 0.98, as shown in Fig. 6.

V. ANALYSIS OF THE SYSTEM DYNAMICS

As seen from Fig. 1(a), a typical array's v–i characteristic is strongly nonlinear. In Fig. 3, the power stage comprises two state variables, and the two differentiators add a further two. Hence, the complete system is described by at least a four-dimensional nonlinear equation of the form $d\mathbf{x}/dt = \mathbf{f}(\mathbf{x}, t)$. This means it has the potential for complex dynamics. Nevertheless, on the basis of a simplified model, we can still derive a two-dimensional mapping which captures the essential features of interest in the behaviour of the real circuit. Details of the derivation can be found in [5]. Due to space constraints, we only present the results here. The approximate stroboscopic mapping is:

$$\left.\begin{aligned} x_{1(k+1)} &= m_2 x_{1(k)} - b_2 x_{2(k)} + c_2 \\ x_{2(k+1)} &= m_3 x_{1(k)} + b_3 x_{2(k)} + c_3 \end{aligned}\right\} \quad \text{if} \quad x_{1(k)} > 1 \qquad (5a)$$

$$\left.\begin{aligned} x_{1(k+1)} &= m_1 x_{1(k)} + a_1 \\ x_{2(k+1)} &= x_{2(k)} - a_2 \end{aligned}\right\} \quad \text{if } x_{1(k)} \le 1 \qquad (5b)$$

where $x_1 = v/V_{mpp}$ and $x_2 = i/I_{mpp}$ are the normalised array voltage and inductor current. With $\beta = CV_{oc}/I_{sc}T_s$, $\alpha = V_b/V_{mpp}$, $\kappa = LI_{sc}/V_{oc}T_s$ and $\tau = t/T_s$ as normalised circuit parameters, we have $m_1 = 1–(1/\beta)(1–1/2\beta)$, $m_2 = 1 – (1/\beta)(1 +1/2\kappa – 1/2\beta)$, $m_3 = (1/\kappa)(1 – 1/2\beta)$, $a_1 = (2/\beta)(1 – 1/2\beta)$, $a_2 = \alpha/\kappa$; $b_2 = (1/\beta)(1 – 1/2\beta)$, $b_3 = 1 – 1/2\beta\kappa$; $c_2 = (2/\beta)(1 + \alpha/4\kappa – 1/2\beta)$, $c_3 = (1/\kappa)((1/\beta) – \alpha)$.

A. The Return Map

We next choose one of the state variables. Here, x_1 was chosen for ease of identifying normalised operation at the MPP, since now $x_{1(mpp)} = 1$. Choosing x_2 produces analogous results. We then plot $x_{1(k+1)}$ against $x_{1(k)}$ to visualise a 1-dimensional return map, as shown in Fig. 7.

The diagonal line $x_{1(k+1)} = x_{1(k)}$ (identity line) divides the graph into two regimes. Equation (5b) lies in the upper regime, describing the evolution of the dynamics when $x_{1(k)} < 1$, implying operation when the switch is open. Because (5b) is uncoupled, the plot of $x_{1(k)}$ against $x_{1(k+1)}$ always exhibits a straight line. Since typically $\beta >> 1$, the slope is typically close to unity.

On the other hand, (5a) lies in the bottom regime. It describes the operation when the switch is closed, since $x_{1(k)} < 1$. However, because (5a) is now coupled, the evolution of $x_{1(k)}$ is also dependent on x_2 and the term $bx_2 + c$ appears as a shifting y-intercept associated with each iteration. If x_2 varies significantly, then a 'fuzzy' region of dots is seen; if not, an almost straight line is exhibited. The latter is assumed in Fig. 9 for the purpose of illustration.

B. A Global Attractor

There are two attracting and stable fixed points (denoted with a superscript asterisk), at $x_1^* = \alpha < 1$ from (5a) and $x_2^* = 2$ from (5b). Because (5b) is valid only in the range $x_{1(k)} \in (\alpha,1]$, and (5a) in the range $x_{1(k)} \in (1,2]$, $\{x_1^*\}$ are virtual fixed points. Note that the union of the two ranges spans the whole operating space for x_1.

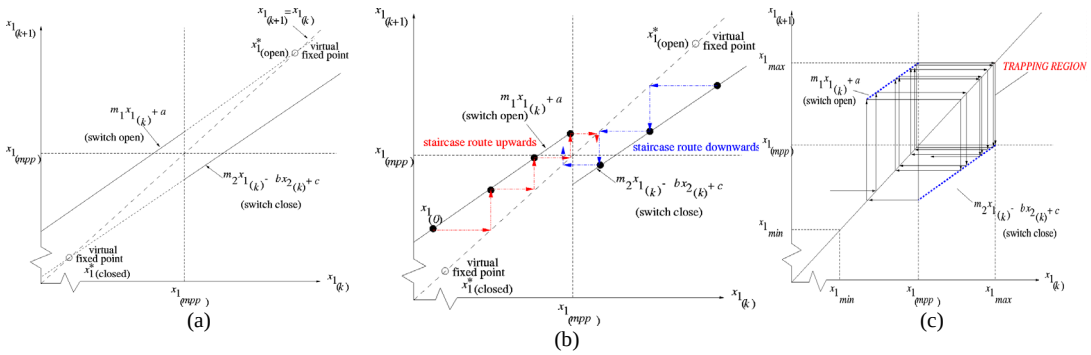

Fig. 7: (a) A return map (showing virtual fixed points); (b) a global attractor; (c) a trapping region

Assume first an initial arbitrary value $x_{1(0)} < 1$. If $x_{1(k)} < 1$, then we are considering only (5b). Because of the virtual fixed point at $x_{1(\text{open})}^{*} = 2$, as long as $x_{1(k)} < 1$, subsequent iterates (marked by a filled dot) will be attracted towards this point. Graphically, the new iterates evolve via a 'staircase' route upwards as shown in Fig. 7(b).

However, if instead $x_{1(k)} > 1$, then (5a) is only considered since the switch is now closed. The only virtual fixed point which is also attracting is now instead at $x_{1(\text{closed})}^{*} = \alpha < 1$. Hence, the sequence of evolving iterates now leads a 'staircase' route downwards.

When the overall picture is considered, any values appearing smaller or greater than the line $x_{(k+1)} = 1$ will be propelled towards it, resulting in a global attractor.

C. *A Trapping Region*

A fixed point cannot exist because the identity line does not intersect either (5a) or (5b), so the system never settles to an equilibrium.

Instead, there exists a trapping region bounded by the limits denoted $x_{1(max)}$ and $x_{1(min)}$ as shown in Fig. 7(c). Once entered, the motion is confined within this region and cannot escape.

The widths of x_1 and x_2, denoted Δx_1 and Δx_2 respectively, define the size of the attractor and are given by

$$\begin{aligned} \Delta x_1 &= \left| \frac{1}{2\beta\kappa}\left(x_{1(mpp)} - \alpha\right) + \frac{1}{\beta}\left(1 - \frac{1}{2\beta}\right) x_{2(mpp)} \right| \\ \Delta x_2 &= \left| \frac{1}{\kappa}\left(1 - \frac{1}{2\beta}\right) x_{1(mpp)} - \frac{1}{\beta\kappa}\left(\frac{x_{2(mpp)}}{2} - 1\right) \right| \end{aligned} \tag{6}$$

From (6), we note that the size of the attractor is affected by the normalised parameters β and κ. The larger the values of β and κ, the smaller the trapping region, and the closer to

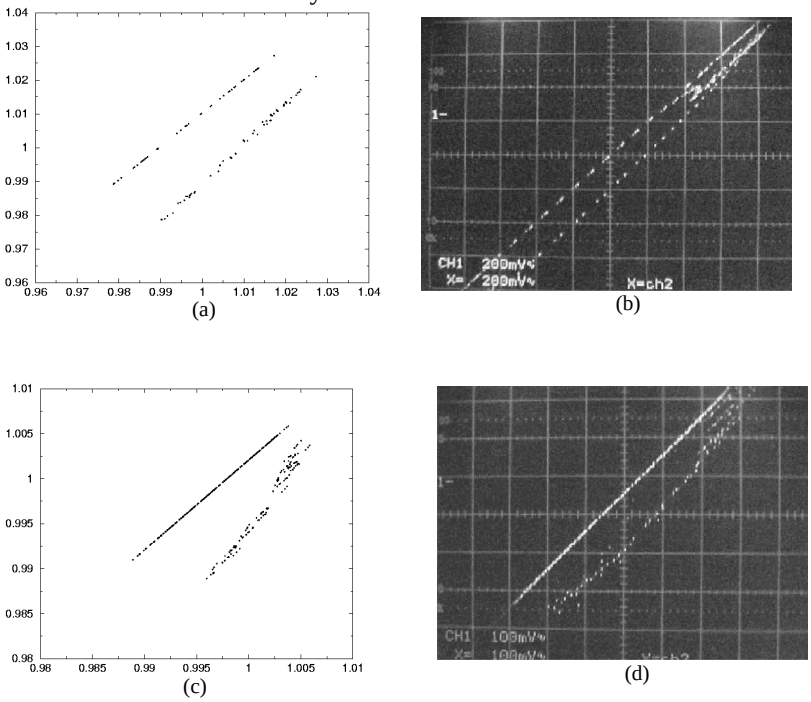

Fig. 8 (a) Simulated (b) Experimental return based on $I_{sc} = 0.75$A and $n_s = 12$; (c) Simulated (d) Experimental return map based on $I_{sc} = 0.25$A and $n_s = 20$

the MPP the operation is confined, yielding a higher tracking effectiveness.

Two experimental return maps based on different operating conditions are shown in Fig. 8(b) and Fig. 8(d). The two operating domains are clearly displayed. In both maps, the upper regions exhibit dotted straight lines, and identify operation where the switch is open. The operation where the switch is closed is highlighted in the lower regions. Due to a lower n_s, the inductor current ripple is much higher, and the term $bx_2 + c$ varies substantially, causing a 'fuzzy' region to appear in Fig. 8 (b). However, with a much higher n_s, $bx_2 + c$ remains relatively constant and instead, the lower region in Fig. 8(d) reveals an approximate straight line.

The existence of a trapping region is not immediately apparent because of the use of practical differentiators. They can be shown in [5] to approximate a perfect differentiator followed by a delay or lag. Hence, curves that define the individual switch operation do not end abruptly at $x_{1(mpp)}$, but we witness an overlap of the slopes. The overlap indicates that during this time, the operation remains in the incorrect switch position due to the delay. However, the preservation of its basic features shows that the attractor remains robust.

Denoting $\phi = T_d/T_s$ as the normalised differentiator time constant, it can be shown that in the limit as $\phi/\beta \rightarrow 0$, perfect differentiators are realised. Given a large β, the effect of the differentiator time constant is minimised. The excursion of x_1 from the MPP can be restricted, and hence the tracking effectiveness improved, by reducing the size of the attractor. This is ensured by the design guidelines $\beta\kappa >> 1$ and $\beta >> 1$.

VI. CONCLUSION

In summary, we propose a new MPPT which employs a simple control strategy from nonlinear dynamics theory. It facilitates autonomous MPP tracking without knowledge of the array characteristics. The controller is simple to implement with a few commonplace electronic building blocks. Experiments based on the parameters used show excellent tracking effectiveness and dynamic response. The controller was also successfully simulated with PSpice using a boost converter, suggesting that this algorithm may be adapted for other dc-dc switching topologies, making it very flexible. Further work will be presented in a planned future paper.

REFERENCES

[1] C.R. Sullivan and M.J. Powers, "A high-efficiency maximum power point tracker for photovoltaic arrays in a solar-powered race vehicle", *Power Electronics Specialists Conf.*, pp. 574–580, June 1993.

[2] T. Hoshino and M. Osakada, "Maximum photovoltaic power tracking, an algorithm for rapidly changing atmospheric conditions", *IEE Proc. Gener. Transm. Distrib.*, vol. 142, no. 1, January 1995.

[3] P. Midya, P.T. Krein, R.J. Turnbull, R. Reppa and J. Kimball, "Dynamic maximum power point tracker for photovoltaic applications", *Power Electronics Specialists Conf.*, vol. 2, pp. 1710–1716, June 1996.

[4] A. Brambilla, M. Gambarara, A. Garutti and F. Ronchi, "New approach to photovoltaic arrays maximum power point tracking", *Power Electronics Specialists Conf.*, June 1999.

[5] Yan Hong Lim, "Nonlinear dynamics of spacecraft power systems", PhD thesis, University of Surrey, UK, November 2000.